Electronic Supplementary Information

Insights Into the Electrochemical Performances of Bi Anodes for Mg Ion Batteries Using ^{25}Mg Solid State NMR Spectroscopy

Zigeng Liu[a], Jeongjae Lee[a], Guolei Xiang[a], Hugh F. J. Glass[a,b], Evan N. Keyzer[a], Siân E. Dutton[b], and Clare P. Grey[a]*

a Department of Chemistry, University of Cambridge, Cambridge, CB2 1EW, UK

b Cavendish Laboratory, University of Cambridge, Cambridge, CB3 0HE, UK

E-mail: cpg27@cam.ac.uk

Experimental section

Material preparation. Bi nanowires were synthesised via a two-step method as described elsewhere.[1] Typically $BiCl_3$ (2 mmol, 98 %, Sigma Aldrich) was dissolved in deionized water (50 mL) under dynamic stirring to form a white precipitate, then Zn powder (4 mmol, 98 %, Sigma Aldrich) was slowly added into the precipitate and the mixture was continuously stirred for 4 h at room temperature. Finally, the mixture was filtered, washed with HCl (1M) and ethanol for 3 times, and dried in a vacuum oven at 60 °C for 3 h to get the final product.

Ball milled Mg_3Bi_2 was prepared by high-energy ball milling of Mg (99 %, Sigma Aldrich) and Bi (99 %, Sigma Aldrich) powders in the 2:1 molar ratio in a ZrO_2 ball mill jar in an Ar atmosphere for 6 hours. Typically, excess Mg is needed for mechanical alloying Mg and Bi to compensate the Mg loss during the ball-milling process (Mg sticking to the balls and ball mill jar).[2,3]

Fabrication of Bi electrode. Bi electrodes were fabricated via a self-supporting film method. A slurry was prepared by mixing 72 wt % Bi, 19 wt % polyvinylidene fluoride (PVDF, Kynar) binder, 9 wt % super P carbon (Timcal) and 5 drops of dibutylphthalate (DBP, Sigma Aldrich) in acetone. Then the slurry was cast onto a glass surface and spread using a 150 μm doctor blade to form a self-supporting film. The film was washed with diethyl ether to remove DBP after cutting into disks with 15 mm diameter. The final film was dried at 100 °C under vacuum for 3 hours and transferred into an Ar filled glove box.

Battery assembly. Coin-type batteries were assembled inside an Ar filled glove box using standard 2032 coin cells (Hohsen Corp.) by stacking the self-supporting film on top of a stainless steel current collector, followed by a glass fiber as separator and Mg ribbon (Sigma Aldrich), polished by a blade, as the counter electrode. A 0.25 M solution of $Mg(AlCl_2EtBu)_2$ in dry THF (stored over activated molecular sieves in an Ar-filled glove box, Sigma Aldrich) was prepared and used as the electrolyte. The cell was pressed closed, the excess electrolyte wiped and rested for 3 hours before cycling. The electrochemical measurement was performed on a Lanhe battery cycler (Wuhan Land Electronics Co. Ltd.) between 0.05 and 0.6V.

Transmission Electron Microscopy (TEM). Morphology of the Bi nanowires was characterized by TEM using a FEI Tecnai G2 F20 instrument operated at 200 kV.

X-ray Diffraction (XRD). Synchrotron XRD patterns were collected in transmission geometry at beamline I11 of the Diamond Light Source using a wavelength of 0.825868 Å and a spot size of 2.5 x 0.5 mm. Samples were mounted into 0.3 mm capillaries. A position sensitive detector (Mythen) was used. Each pattern was collected for 30 seconds.

Rietveld analysis was performed using the FullProf suite over a 2θ range of 10°-92°, with a step size of 2θ = 0.003998°.[4,5] Backgrounds were fit using a linear interpolation of data points. The peak shape was modelled using a pseudo-Voigt function and peak broadening was modelled using a symmetry dependent Scherrer analysis.[6] This analysis uses a spherical harmonic expansion dependent on the Laue class of the crystal. Micro-particle size is then inferred by comparison with the peak widths of a crystalline silicon standard.

In situ XRD data were collected on a Panalytical Empyrean diffractometer using a Cu Kα radiation, λ ~1.542 Å, at room temperature. Scans were collected over 30 minutes over the angular range $30 \leq 2\theta \leq 50^{o}$ with $\Delta 2\theta = 0.0167^{o}$. A modified Swagelok battery, with a Be disk window was used for the in situ XRD measurements. The electrochemical cycling current rate was 12.8 mA/g.

Solid-state nuclear magnetic resonance (ssNMR). ^{25}Mg ssNMR spectra were acquired on a Bruker AVIII-700 spectrometer, at a ^{25}Mg Larmor frequency of 42 MHz. Variable temperature experiments on electrochemical prepared Mg_3Bi_2 were used a Bruker 3.2 mm triple resonance probe, spinning at 20 kHz. The other room temperature and variable temperature experiments were carried out using a Bruker 4 mm triple resonance probe, spinning at 14 kHz frequency. All experiments employed a rotor-synchronised Hahn-echo pulse sequence with 90° pulse length of 2.8 μs, recycle delay of 20 ms. Around 50 mg of sample was used in each experiment, with the number of scans varying from 409600 to 2048000 depending on the S/N observed. Intensities were normalised to the respective number of scans. ^{25}Mg shifts were referenced to MgO powder secondary reference (26 ppm).

Spectral fit. The measured spectra were fit using a two-site exchange model as implemented in the MEXICO code.[7] Fixed linewidths of 500 and 2000 Hz were applied to the fast and slow moving component of the spectra, respectively. As an automated fit failed to converge, each spectra was fit by manually changing the exchange frequency until the fitted spectrum showed reasonable agreement to the experimental spectrum.

Supporting figures and tables

Galvanostatic charge/discharge data

As discussed in the main text, the large difference between the first discharge and charge capacity of the cell cycled at a rate corresponding to C/2 (shown in Figure 2a) is primarily due to some electrolyte breakdown on the first discharge. This phenomenon is coupled with the difficulty in breaking up the relatively large pristine Bi nanowires and the nucleation and growth of a new phase (Mg_3Bi_2) that is not structurally related to the original one, particularly when a relatively fast cycling rate of C/2 is used. This latter suggestion is confirmed by observations that the first discharge (i) has the greatest overpotential, and (ii) is associated with a classic nucleation dip (the voltage dropping to almost 0.08 V, before increasing again). Only 285 $mAhg^{-1}$ can be recovered in the 1st charge. A combination of electrochemical grinding and residual Mg_3Bi_2 nanoparticles, which presumably act as nucleation sites for further Mg_3Bi_2 formation, results in a noticeably lower overpotential on the second discharge and a capacity that is slightly over the theoretical value (again indicating some electrolyte breakdown). The capacity on charge increases indicating that more Mg_3Bi_2 has been formed on the second discharge than in the first. The overpotential drops further as cycling continues and the material cycles with an increasingly higher coulombic efficiency. A stable passivating layer appears to have formed at this point that prevents further electrolyte breakdown and does not hinder reaction with Mg^{2+} accounting for the increase in coulombic efficiency. The coulombic efficiency is close to 100% after 10 cycles. When the cycling rate is reduced to C/20, the high overpotential and nucleation dip are similarly observed in the 1st discharge; however the capacity of 1st charge is now larger (approximately 353 $mAhg^{-1}$), the charge capacity remaining the same in the subsequent cycles. This indicates that the full capacity can be achieved and a stable passivation layer can be formed in the first cycle at this lower rate.

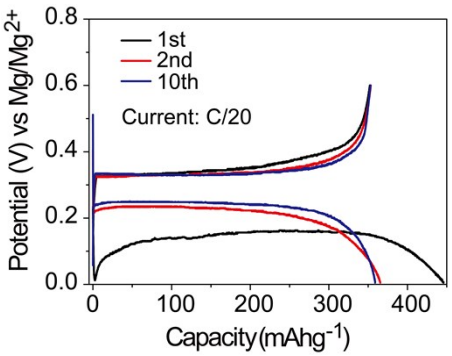

Figure S1. The charge-discharge profile of a Bi/Mg cell at a rate of C/20 with a Grignard electrolyte.

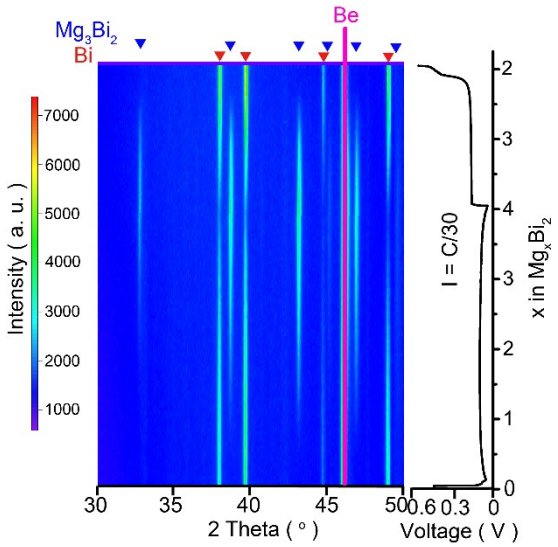

Figure S2. Contour plot showing the in situ XRD patterns obtained for the Bi anode during discharge and charge, obtained using a laboratory X-ray source. The reflections due to Bi, Mg_3Bi_2 and Be disk are marked with red triangles, blue triangles and a solid pink line, respectively. The electrochemistry profile for this battery (cycled at current density of 12.8 mA/g, corresponding to C/30 rate) is shown on the right hand side.

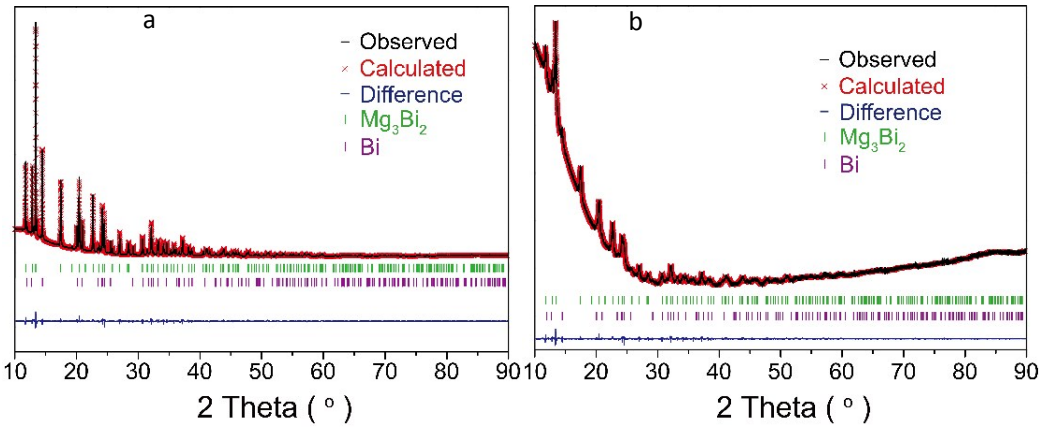

Figure S3. Rietveld refinement of the synchrotron XRD patterns of Mg_3Bi_2 synthesised by electrochemical (a) and mechanical alloying (b).

Table S1. Lattice parameters and particle sizes from synchrotron X-ray diffraction of Mg_3Bi_2 prepared *via* electrochemical and mechanical alloying methods. Phase fraction of excess Bi is given; the remaining phase fraction corresponds to Mg_3Bi_2. Particle sizes were determined via a Scherrer analysis.

Mg_3Bi_2 Space group = $P\bar{3}m1$			
		Electrochemical alloying	Mechanical alloying
a (Å)		4.65432(1)	4.65289(9)
b (Å)		4.65432(1)	4.65289(9)
c (Å)		7.38749(2)	7.3883(2)
R_{wp} (%)		8.59	13.9
Particle size (nm)		55.3	9.5
Bi (wt %)		18.4(7)	10.5(5)
Site positions			
Bi 2d (1/3, 2/3, z)	z B_{iso} (Å^2)	0.22378(8) 2.122(10)	0.22263(20) 1.18 (3)
Mg 1 1a (0, 0, 0)	B_{iso} (Å^2)	1.48 (13)	1.9 (5)
Mg 2 2d (1/3, 2/3, z)	z B_{iso} (Å^2)	0.6310(4) 1.99(8)	0.6274(14) 1.7(2)

Analysis of Mg motion

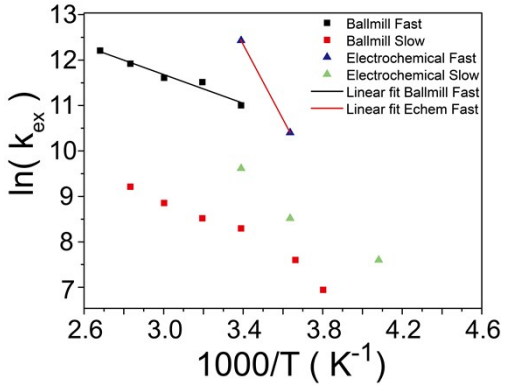

Figure S4. Arrhenius plot of the exchange rates (k_{ex}) between the two Mg sites versus 1000/T for both electrochemically and mechanically prepared Mg_3Bi_2 samples.

It is not straightforward to extract an activation barrier for Mg transport based on the NMR data as discussed below. A simple Arrhenius analysis comprising ln (k_{ex}) plotted as a function of inverse temperature (1000/T) (Figure S3a) for the Mg^{2+} ions in both the slow and fast regimes for both mechanically and electrochemically prepared Mg_3Bi_2. Although the relative populations of the Mg^{2+} ions in the slow and fast regime changes with temperature, linear fits are seen for both subsets of spins for the ball-milled sample, where more data points are available, leading to *apparent* activation energy values of the fast Mg ions transport of 0.19 eV (and similar for the slow moving Mg ions). Much higher *apparent* activation energies, albeit with limited data points, are extracted from the electrochemically prepared sample (0.71 eV). The meaning of these activation energies must however be questioned. Considering the fast moving subset of ions only, our simple fits to the data provide a measure of the fraction of spins undergoing Mg1-Mg2 hops with an average frequency given by k_{ex}. However, the fraction of spins in this fast regime also changes with temperature and so the activation energy measured via a plot of ln(k_{ex}) also contains an activation energy associated with an increase in the mobile fraction of carriers (technically the Mg^{2+} vacancies, but observed here indirectly via the Mg^{2+} ions). We are currently developing a more detailed model of motion in this system to account for the distribution of correlation times. Conductivity measurements are also in progress to explore this phenomenon and to explore the relationship between short-range motion probed by NMR spectroscopy and long-range Mg^{2+} transport. What is clear however is that Mg^{2+} transport at room temperature is extremely rapid, particularly for samples prepared electrochemically.

References

1 B. Yang, C. Li, H. Hu, X. Yang, Q. Li and Y. Qian, *Eur. J. Inorg. Chem.*, 2003, **20**, 3699–3702.

2 H. X. Xin, X. Y. Qin, X. G. Zhu, J. Zhang and M. G. Kong, *Mater. Sci. Eng. B Solid-State Mater. Adv. Technol.*, 2006, **128**, 192–200.

3 F. Murgia, L. Stievano, L. Monconduit and R. Berthelot, *J. Mater. Chem. A*, 2015, **3**, 16478–16485.

4 H. M. Rietveld, *J. Appl. Crystallogr.*, 1969, **2**, 65–71.

5 J. Rodriguez-Carvajal, *Phys. B Phys. Condens. Matter*, 1993, **192**, 55–69.

6 P. Scherrer, *Nachrichten von der Gesellschaft der Wissenschaften zu Göttingen, Math. Klasse*, 1918, **2**,

98–100.

7 A. D. Bain and G. J. Duns, *Can. J. Chem.*, 1996, **824**, 819–824.

8 F. Zhang, Y. Tang, B. Hu, S. Liu, Y. Du and Y. Zhang, *J. Min. Metall. Sect. B Metall.*, 2014, **50**, 115-126.